BIOCHEMISTRY
including biophysical chemistry & molecular biology

Article

pubs.acs.org/biochemistry

Tryptophan 697 Modulates Hydride and Interflavin Electron Transfer in Human Methionine Synthase Reductase

Carla E. Meints,[†] Frida S. Gustafsson,[†] Nigel S. Scrutton,[‡] and Kirsten R. Wolthers*[,†]

[†]Department of Chemistry, University of British Columbia, 3333 University Way, Kelowna, BC, Canada V1V 1V7

[‡]Manchester Interdisciplinary Biocentre, Faculty of Life Sciences, University of Manchester, 131 Princess Street, Manchester M1 7DN, U.K.

ABSTRACT: Human methionine synthase reductase (MSR), a diflavin oxidoreductase, plays a vital role in methionine and folate metabolism by sustaining methionine synthase (MS) activity. MSR catalyzes the oxidation of NADPH and shuttles electrons via its FAD and FMN cofactors to inactive MS-cob(II)alamin. A conserved aromatic residue (Trp697) positioned next to the FAD isoalloxazine ring controls nicotinamide binding and catalysis in related flavoproteins. We created four MSR mutants (W697S, W697H, S698Δ, and S698A) and studied their associated kinetic behavior. Multiwavelength stopped-flow analysis reveals that NADPH reduction of the C-terminal Ser698 mutants occurs in three resolvable kinetic steps encompassing transfer of a hydride ion to FAD, semiquinone formation (indicating FAD to FMN electron transfer), and slow flavin reduction by a second molecule of NADPH. Corresponding experiments with the W697 mutants show a two-step flavin reduction without an observable semiquinone intermediate, indicating that W697 supports FAD to FMN electron transfer. Accelerated rates of FAD reduction, steady-state cytochrome c^{3+} turnover, and uncoupled NADPH oxidation in the S698Δ and W697H mutants may be attributed to a decrease in the energy barrier for displacement of W697 by NADPH. Binding of $NADP^+$, but not 2′,5′-ADP, is tighter for all mutants than for native MSR. The combined studies demonstrate that while W697 attenuates hydride transfer, it ensures coenzyme selectivity and accelerates FAD to FMN electron transfer. Moreover, analysis of analogous cytochrome P450 reductase (CPR) variants points to key differences in the driving force for flavin reduction and suggests that the conserved FAD stacking tryptophan residue in CPR also promotes interflavin electron transfer.

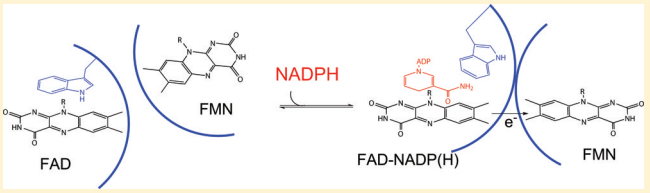

Vitamin B_{12} (cobalamin)-requiring enzymes from both microbes and mammals are susceptible to inactivation because of the spurious oxidation of the B_{12} cofactor during catalytic turnover.[1,2] Several auxiliary enzymes that function to repair or replace the damaged cobalamin cofactor have been identified, but the detailed mechanism by which they act or their overall influence on the metabolic output of the B_{12} enzyme is not fully understood.[3−5] A case in point is human cobalamin-dependent methionine synthase (MS) and its reactivating enzyme, methionine synthase reductase (MSR); knowledge of their biochemical relationship is critical to human health as they are key enzymes in the cellular processing of homocysteine and N^5-methyl-tetrahydrofolate.

The importance of MS and MSR to one-carbon metabolism and cell homeostasis is illustrated in their overlapping catalytic cycles (Figure 1). MS recycles homocysteine through methylation of the thiol side chain, generating methionine. Methionine can subsequently be used in protein synthesis or serve as a precursor in the biosynthesis of *S*-adenosylmethionine, a methyl donor for a vast number of cellular processes (DNA, RNA, and protein methylation, neurotransmitter biosynthesis). MS also demethylates N^5-methyl-tetrahydrofolate to form tetrahydrofolate, an important metabolite for the purine and thymidylate biosynthetic pathways. MS-bound cobalamin acts as an intermediary in the two transmethylation reactions and cycles between the methylcob(III)alamin and cob(I)alamin states during turnover.[6] It is the latter, highly nucleophilic form of the cofactor that is susceptible to one-electron oxidation, producing cob(II)alamin. The event, which occurs every ∼2000 catalytic turnovers, renders MS inactive.[1] MSR, a 78 kDa diflavin oxidoreductase, binds to inactive MS-cob(II)alamin through its FMN-containing domain.[7,8] It transfers an electron derived from the oxidation of NADPH via its FAD and FMN cofactors to the Co^{2+} metal center of cob(II)alamin. MSR-catalyzed reduction of cob(II)alamin is coupled to the transfer of a methyl group from *S*-adenosylmethionine to generate active MS-methylcob(III)-alamin.

MSR's crucial role in sustaining MS function is evident in individuals with genetic deficiencies in the enzyme. Inborn errors of MSR constitute a rare autosomal recessive disorder, resulting in high levels of plasma homocysteine (hyperhomocysteinemia) and megaloblastic anemia.[9] Patients may suffer from a variety of neurological deficits, including developmental delay, blindness, and cerebral atrophy.[10]

Received: August 5, 2011
Revised: November 16, 2011
Published: November 18, 2011

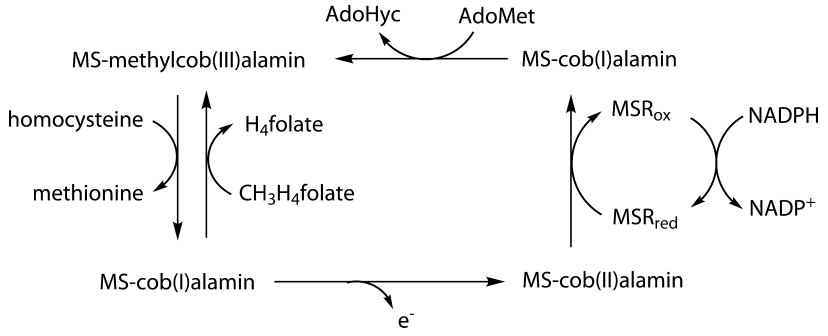

Figure 1. Complete catalytic cycle of methionine synthase. MS-cob(I)alamin is formed following transfer of a methyl group from MS-methylcob(III)alamin to homocysteine forming methionine. CH_3H_4folate subsequently transmethylates MS-cob(I)alamin, generating H_4folate and MS-methylcob(III)alamin. Occasional oxidation of MS-cob(I)alamin generates catalytically inert MS-cob(II)alamin. Active MS-methylcob(III)-alamin is restored with donation of an electron from the reduced FMN center of MSR and the transfer of a methyl group from *S*-adenosylmethionine.

Elevated levels of plasma homocysteine also constitute a risk factor for Alzheimer's, cardiovascular disease, and neural tube defects.[11−13] A common polymorphism of MSR, which has a modest impact on MS reactivation, confers a risk factor for women bearing children with neural tube defects; for women with low levels of serum cobalamin, this risk factor is elevated.[14,15] A mouse model that is a hypomorphic mutant for MSR has high levels of plasma homocysteine and is more prone to bearing offspring with birth defects.[16,17] These clinical and animal studies clearly establish that the catalytic integrity of MSR is acutely tied to MS function.

On the basis of amino acid sequence and diflavin topology, MSR seemingly arose from the genetic fusion of two bacterial flavoproteins that comprise the reactivation mechanism for the *Escherichia coli* homologue of human cobalamin-dependent methionine synthase (MetH). In *E. coli*, an FAD-containing ferredoxin NADP(H) oxidoreductase (FNR) catalyzes the oxidation of NADPH and delivers an electron to an FMN-containing flavodoxin (Fld), which then relays the electron to inactive MetH.[18,19] The N- and C-termini of MSR are structurally related to bacterial Fld and FNR, respectively, and these domains are fused by an additional connecting domain and flexible hinge. This diflavin structural design is also observed in other mammalian NADPH-dependent oxidoreductases, cytochrome P450 reductase (CPR),[20] the reductase component of the nitric oxide synthases (NOSred),[21] and NADPH-dependent oxidoreductase 1 (NR1).[22] A distinctive feature of MSR is an 82-amino acid stretch that tethers the FMN domain to the connecting domain. This stretch of polypeptide maps to a flexible 15−24-amino acid hinge in CPR and NOSred that allows for intra- and interprotein electron transfer by conferring conformational freedom of the FMN domain.[23,24]

While the overall sequence of hydride and electron transfer is the same for the diflavin oxidoreductases (i.e., NADPH → FAD → FMN), studies from various groups have revealed sharp differences in their overall kinetic behavior.[25,26] Stopped-flow analysis of NADPH-mediated reduction of MSR occurs in four resolvable kinetic phases that correspond to rapid and transient formation of a charge transfer complex upon NADPH binding, transfer of a hydride ion to FAD, transfer of an electron from FAD to FMN, and finally full four-electron reduction by a second molecule of NADPH (Figure 2).[27] The time course for the four-electron reduction of MSR is ∼200 s, >100-fold slower than that for CPR[28] and NOSred.[29] The extended time frame

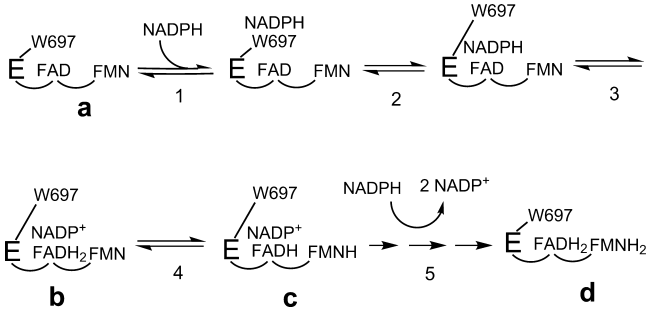

Figure 2. Kinetic scheme for the NADPH-catalyzed reduction of MSR under pseudo-first-order conditions. Step 1 is binding of NADPH to MSR with the flavin cofactors in the fully oxidized state (FAD and FMN). Step 2 is displacement of W697 by the nicotinamide ring of NADPH. Step 3 is transfer of a hydride ion from C4 of the nicotinamide ring to N5 of the FAD isoalloxazine ring, producing the hydroquinone form of the cofactor ($FADH_2$) and $NADP^+$. Step 4 is internal transfer of an electron from $FADH_2$ to FMN producing the semiquinone forms of both cofactors ($FADH^•$ and $FMNH^•$), denoted by an increase in absorbance at 600 nm. Step 5 encompasses multiple steps that involve full four-electron reduction of the enzyme by a second molecule of NADPH. The first observed phase of flavin reduction, k_{obs1}, is influenced by the rates of coenzyme binding, displacement of W697, and hydride transfer.

for complete flavin reduction is partially attributed to slow interflavin electron transfer and may explain the enzyme's slower observed rate for FMN-mediated reduction of the nonphysiological electron acceptor, cytochrome c^{3+}.[7,30] Stopped-flow and isothermal titration calorimetry (ITC) experiments have also demonstrated that coenzyme binding is significantly weaker in MSR than in NOSred and CPR,[27,31] which may help minimize uncoupled NADPH oxidation in an enzyme with limited biological function (reactivation of MS every ∼2000 catalytic turnovers). Weak NADPH binding coupled with a putative thermodynamically unfavorable electron transfer step from the MSR $FMN_{sq/hq}$ redox center to MS-cob(II)alamin[18] and slow interflavin electron transfer may severely restrict MS reactivation and limit folate and homocysteine metabolism.

In this study, we have explored regulatory elements of MSR that control nicotinamide binding and rates of hydride and interflavin electron transfer. We have focused on the last two C-terminal residues, Trp697 and Ser698, located in the coenzyme-binding pocket (Figure 3). On the basis of the full-

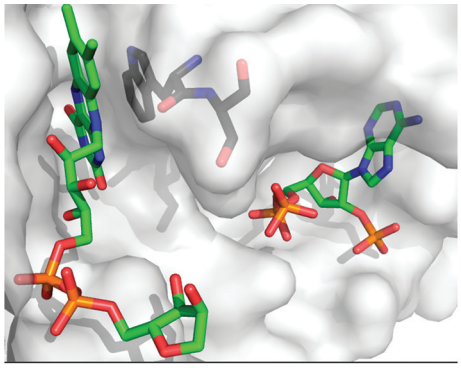

```
Human MSR          691 RYLQDIWS—698
C.elegans MSR      675 QYIEDVWG-- 682
Human CPR          673 RYSLDVWS-- 680
Human NR1          599 RFQTETWA-- 606
Human nNOS        1393 RYHEDIFGVTLRTYEVTNRLRSESIAFIEESKKDTDEVFSS-- 1433
Spinach FNR        308 QWNVEVY--- 314
```

Figure 3. Location of Trp697 and Ser698 in crystal structure of the MSR FNR module (Protein Data Bank entry 2QTZ). Hydrophobic interaction between the indole of W697 (black) and the FAD isoalloxazine ring (green) and the position of the 2′,5′-ADP portion of the $NADP^+$ in the coenzyme-binding cleft are shown. Below is a sequence alignment of human MSR (MSR, Swiss-Prot entry Q90BK8), *Caenorhabditis elegans* MSR (Swiss-Prot entry Q17574), human CPR (Swiss-Prot entry P0038), human nNOS (Swiss-Prot entry P29475), and spinach ferredoxin:$NADP^+$ reductase (Swiss-Prot entry P00455). The conserved aromatic residue is colored red.

length structure of CPR,[20] these residues are part of the binding interface with the FMN domain. The indole side chain of Trp697 forms $\pi-\pi$ stacking interactions with the *re* face of the FAD isoalloxazine ring, and crystallographic studies with FNR[32] and CPR[33] indicate that this conserved aromatic side chain is displaced to allow for optimal positioning of the NADPH nicotinamide ring for the transfer of a hydride ion to FAD. In an effort to reduce the energy barrier for displacement of Trp697 and potentially increase the rates of flavin reduction, W697H and W697S variants of MSR were generated. Creation of these specific W697 mutants provided the opportunity to directly compare our kinetic data with those of analogous mutants of human CPR and neuronal nitric oxide synthase (W676H and F1395S, respectively).[34,35] To determine if the neighboring C-terminal S698 also contributes to the energetic barrier for catalytic placement of the nicotinamide ring, the residue was deleted or substituted for an Ala. Two of the MSR variants (W697H and S698Δ) exhibited not only tighter binding of NADP(H) but also faster rates of hydride transfer and steady-state cytochrome c^{3+} reduction, which may have implications for MS reactivation and primary metabolism. The remaining mutants, S698A and W697S, elicited catalytic properties that were similar and suppressed compared to those of the native enzyme, respectively. Analysis of the combined data suggests a broader role for the FAD aromatic stacking residue in controlling rates of hydride and interflavin electron transfer in diflavin oxidoreductases.

EXPERIMENTAL PROCEDURES

Materials. The reagents NADPH, NADH, $NADP^+$, 2′,5′-ADP, and cytochrome c^{3+} were purchased from Sigma-Aldrich. The Resource Q column and glutathione Sepharose 4B resin were purchased from GE Biosciences. *Pfu* Turbo DNA polymerase and Xl1 Blue cells were from Agilent Technologies, and Rosetta(DE3)pLysS competent cells were from EMD Biosciences. All other chemicals and reagents were purchased from Fisher.

Generation, Expression, and Purification of MSR Mutants. The W697H, W697S, S698A, and S698Δ variants of MSR were generated using the QuikChange Site-Directed Mutagenesis Kit (Agilent Technologies) using the pGEXMSR plasmid as a template.[36] Primers were obtained from Integrated DNA Technologies (Coralville, IA). Sequencing of the MSR variants by the NAPS DNA sequencing laboratory at the University of British Columbia (Vancouver, BC) confirmed that single-amino acid mutations had been successfully generated and that no other polymerase chain reaction-induced errors had been produced. The plasmids harboring the designed mutants of MSR were transformed into the Rosetta2(DE3)pLysS strain of *E. coli*, and recombinant proteins were expressed and purified as previously described.[36] The final protein concentration was calculated from an absorbance reading at 454 nm (extinction coefficient of 25600 M^{-1} cm^{-1}).

Steady-State Turnover Analysis. The rate of MSR-catalyzed reduction of cytochrome c^{3+} was determined at 25 °C by following the absorbance change at 550 nm ($\Delta\varepsilon$ = 21.1 mM^{-1} cm^{-1})[37] on a Lambda 25 UV−visible spectrometer (Perkin-Elmer). The 1 mL reaction mixture contained 50 mM Tris-HCl (pH 7.5) (measured at 22 °C), 8 μM cytochrome c^{3+}, variable NADPH and NADH concentrations, and variable concentrations of inhibitor, $NADP^+$ or 2′,5′-ADP. The reactions were initiated via the addition of MSR. Inhibition data were fit to the equation for competitive inhibition by nonlinear least-squares analysis using Origin version 8.5 (OriginLab Corp.).

$$v_i = \frac{VA}{K_m(1 + I/K_i) + A} \quad (1)$$

where v_i is the initial velocity, V is the maximal velocity, A is the NADPH concentration, K_m is the apparent Michaelis constant for NADPH, I is the inhibitor concentration, and K_i is the inhibition constant. Uncoupled NADPH oxidation was measured at 25 °C in 50 mM Tris-HCl (pH 7.5) and 1 mM NADPH. The initial velocity was calculated from an absorbance change at 340 nm using an extinction coefficient of 6.22 mM^{-1} cm^{-1}.

Stopped-Flow Kinetic Measurements. Single-turnover pre-steady-state kinetic measurements were performed under anaerobic conditions using the SF-61DX2 stopped-flow system

Table 1. Kinetic and Inhibition Constants for Wild-Type and Mutant MSR-Catalyzed Reduction of Cytochrome c^{3+} with NADPH

MSR	inhibitor	k_{cat} (s^{-1})	K_{NADPH} ($\times 10^{-6}$ M)	K_i ($\times 10^{-6}$ M)	k_{cat}/K_m ($\times 10^{-6}$ M^{-1} s^{-1})
S698Δ	$NADP^+$	12.2 ± 0.4	1.9 ± 0.2	2.2 ± 0.3	6.2 ± 0.8
	2′,5′-ADP	13.9 ± 0.5	2.7 ± 0.3	0.5 ± 0.1	5.2 ± 0.8
S698A	$NADP^+$	3.2 ± 0.3	4.6 ± 1.1	9.2 ± 1.9	0.7 ± 0.2
	2′,5′-ADP	2.6 ± 0.1	5.6 ± 0.8	0.4 ± 0.1	0.5 ± 0.1
W697S	$NADP^+$	0.64 ± 0.02	0.25 ± 0.06	0.09 ± 0.02	2.6 ± 0.7
	2′,5′-ADP	0.69 ± 0.01	0.44 ± 0.06	2.4 ± 0.5	1.6 ± 0.2
W697H	$NADP^+$	15.3 ± 0.6	4.0 ± 0.5	25.6 ± 4.9	3.8 ± 0.6
	2′,5′-ADP	18.3 ± 0.5	3.8 ± 0.3	1.9 ± 0.1	4.8 ± 0.5
wild type[a]	$NADP^+$	7.2 ± 0.1	2.4 ± 0.2	36.9 ± 2.7	3.1 ± 0.3
	2′,5′-ADP	6.6 ± 0.1	2.0 ± 0.1	1.4 ± 0.1	3.4 ± 0.3

[a]Data from ref 31.

(TgK Scientific) in a customized glovebox (Belle Technology) in which the concentration of O_2 was <5 ppm. Measurements were performed at 25 °C in 50 mM Tris-HCl (pH 7.5) (measured at 22 °C) that was made free of O_2 by being extensively bubbled with nitrogen gas followed by equilibration for >16 h in the glovebox. Concentrated protein samples (1−2 mL) were brought into the glovebox, and oxygen was removed by gel filtration over a 10 mL Bio-Rad Econo-Pac DG column equilibrated with anaerobic buffer. Solid NADPH was introduced into the glovebox and dissolved in anaerobic buffer.

Stopped-flow multiwavelength absorption studies were conducted with a photodiode array detector (PDA). Excess NADPH (400 μM) was mixed with an equal volume of 20 μM MSR, and spectral changes were recorded over 200−500 s. The spectral data were exported from Kinetic Studio (TgK Scientific) and evaluated in ReactLab Kinetics (Jplus Consulting Pty Ltd.) by singular-value decomposition (SVD), which allowed for a model-free determination of the number of spectral species that form during the course of the reaction. The reduced SVD data were best fit to a three-step model (A → B → C → D) with four discrete spectral species for the S698 mutants or a two-step model (A → B → C) with three discrete spectral species for the W697 mutants. We also investigated the two-electron reduction of the MSR W697H and W697S mutants by rapidly mixing the enzyme with an equimolar amount of NADPH and recording changes in flavin absorption over 750 s with PDA spectroscopy.

For single-wavelength studies, NADPH reduction of MSR was followed at 454 nm at 25 °C under pseudo-first-order conditions with NADPH in >7-fold excess of enzyme concentration. The substrate and MSR mutant sample (syringe concentration of 8 μM) were both diluted 2-fold after mixing. An average of three traces of the single-wavelength data were fit to a double-exponential equation (eq 2)

$$A = C_1 e^{-k_{obs1}t} + C_2 e^{-k_{obs2}t} + b \quad (2)$$

where k_{obs1} and k_{obs2} are the observed rate constants for the fast and slow phases, respectively, C_1 and C_2 are their relative amplitudes, and b is the final absorbance value.

RESULTS

Characterization of the Mutants. The UV−visible absorbance spectra of the four generated mutants are similar to that of the native enzyme and indicate two flavins bound per polypeptide. In contrast to CPR and NOSred, the MSR variants (including the native enzyme) do not harbor an air-stable FMN semiquinone (a broad absorbance band at 590 nm), despite having similar $FMN_{ox/sq}$ midpoint potentials.[36] The FMN cofactor may be less shielded from the solvent in MSR compared to that of related enzymes, leading to full oxidation of the isoalloxazine ring. Moreover, there is no spectral evidence of the stable formation of a charge transfer complex (signified by an absorbance band above 500 nm) upon addition of saturating amounts of $NADP^+$ to the oxidized MSR variants [including native MSR (data not shown)]. The E−FAD−NADP(H) charge transfer state described for CPR and FNR refers to a precatalytic enzyme−coenzyme complex in which initial docking of the coenzyme leads to a restructuring of the active site.[32,33] The broad absorbance band at >500 nm has been attributed to movement of the FAD aromatic stacking residue with respect to the isoalloxazine ring but can also signify interaction between the nicotinamide ring and an active site residue or FAD.[25]

Steady-State Kinetic Analysis. Initially, steady-state cytochrome c^{3+} assays were used to access the overall kinetic performance of the MSR variants. The advantage of using cytochrome c^{3+} as an electron acceptor is twofold. First, it is a universal electron acceptor for all diflavin oxidoreductases, allowing for direct comparisons between family members. Second, reduction of cytochrome c^{3+} occurs through donation of an electron from the FMN redox center; therefore, k_{cat} is a product of all forward catalytic steps of the mechanism, including NADPH binding, transfer of a hydride to FAD, FAD to FMN electron transfer, and dissociation of $NADP^+$ (Figure 2). The k_{cat} for MSR-catalyzed cytochrome c^{3+} reduction is 1−6 s^{-1},[7,31] similar to that of NR1.[22] By comparison, mammalian CPR elicits turnover numbers between 50 and 80 s^{-1},[30] while NOSred activity varies between 3 and 50 s^{-1} depending on the isoform and the presence or absence of calmodulin.[38] As shown in Table 1, W697H showed the highest k_{cat} for cytochrome c^{3+} reduction (~15 s^{-1}), a 2-fold increase over that of wild-type MSR, followed by S698Δ (~12 s^{-1}), S698A (3 s^{-1}), and W697S (0.6 s^{-1}). The enzyme specificity (k_{cat}/K_m) for NADPH did not differ significantly from that of the native enzyme, except in the S698A mutant, which displayed a 6-fold reduction in k_{cat}/K_m. Steady-state inhibition studies with $NADP^+$ and 2′,5′-ADP were also performed to investigate if the single-point mutations affect the binding of oxidized coenzyme and/or substrate analogue. All product and dead-end inhibition data were fit to an equation for competitive inhibition (eq 1). For 2′,5′-ADP, which lacks the nicotinamide mononucleotide (NMN) portion of the coenzyme, the K_i ranges between 0.4 and 2.4 μM, values close to that observed for the wild type. By

dx.doi.org/10.1021/bi2012228 | Biochemistry 2011, 50, 11131−11142

contrast, the inhibition constant for $NADP^+$ varies significantly for each of the variants tested, but they all fall below that of the native enzyme (37 μM).[31] W697S, which has the slowest rate of cytochrome c^{3+} reduction, showed the tightest binding affinity for $NADP^+$ (K_i = 0.09 μM), >400-fold higher than that of wild-type MSR. S698Δ also elicited a low K_i for $NADP^+$ (2 μM), followed by S698A (9 μM) and W697H (25 μM).

Uncoupled NADPH Oxidation. The rate of uncoupled NADPH oxidation was measured to pinpoint steps in the catalytic mechanism that may be affected by the mutants. MSR-catalyzed oxidation of NADPH leads to the formation of reduced flavins, which are then returned to the fully oxidized state by donation of an electron to O_2. In these assays, interflavin electron transfer does not limit NADPH turnover, as reduced $FADH_2$ can also be reoxidized by molecular O_2. As shown in Figure 4, there was an 8−10-fold increase in the level

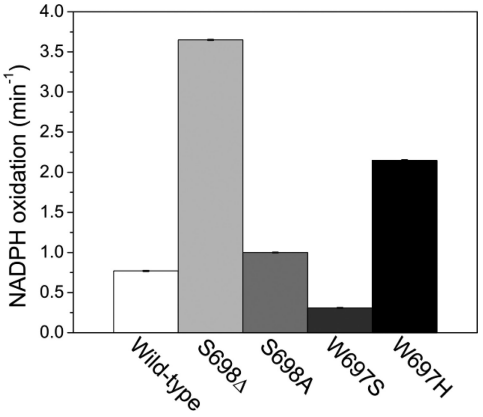

Figure 4. NADPH oxidase activity of MSR variants. Histogram showing uncoupled NADPH turnover by the four mutants of MSR. Kinetic assays are described in Experimental Procedures.

of uncoupled NADPH oxidation in the S698Δ and W697H mutants compared to the native enzyme, while S698A and W697S showed attenuated rates of coenzyme turnover (50% of that of the wild type enzyme). These data partially mirror steady-state cytochrome c^{3+} reduction in that deletion of the terminal Ser residue or conversion of the W697 indole side chain to an imidazole moiety accelerates catalysis. A more pronounced effect on turnover for uncoupled NADPH oxidation suggests that enhanced catalytic performance is attributed to more efficient hydride transfer in S698Δ and W697H, as opposed to improved rates of interflavin electron transfer, a catalytic step that is required for cytochrome c^{3+} reduction.

Multiwavelength Stopped-Flow Analysis of Flavin Reduction. Stopped-flow analysis was performed on the MSR variants to further resolve step(s) in the catalytic cycle (hydride transfer and $FADH_2$ to FMN electron donation) that account for differences in steady-state turnover. As with wild-type MSR, pre-steady-state analysis of flavin reduction was performed by both multiwavelength and single-wavelength stopped-flow analysis to allow assignment of observed kinetic phases to mechanistic steps in the reductive half-reaction. For multiwavelength analysis, a photodiode array detector was used to record UV−visible spectra from 300 to 700 nm over a select time domain. Each MSR variant was rapidly mixed with a 10-fold excess of NADPH under anaerobic conditions, and the spectra were recorded every 1.8 ms. Bleaching of the flavin absorbance occurred between 200 and 500 s, and the time-resolved spectra from 380 to 700 nm were processed by singular-value decomposition (SVD) with ReactLab. For the two Ser698 mutants, the SVD-transformed data were best fit to a three-step irreversible model with four spectral species (A → B → C → D), similar to that of wild-type MSR, whereas data for the W697 mutants were best fit to a two-step model with three spectral species (A → B → C). Global fitting of these models to the SVD-processed data generated spectral profiles for each of the intermediates and observed rate constants for their formation and decay during the time course of the reaction (Figure 5 and Table 2). It should be noted that the spectral intermediates (A−D) are a distribution of enzyme intermediates that form within a resolvable kinetic phase.

The first kinetic phase observed for all four mutants is the conversion of species A (the fully oxidized enzyme) to spectral intermediate B. The spectra of B for all four mutants show a partial reduction in the absorbance maxima at 454 nm, without an increase in absorbance at 600 nm. On the basis of the spectral signature of B, the first kinetic phase (k_{obs1}) encompasses the first hydride transfer step from NADPH leading to formation of the two-electron-reduced state [E−$FADH_2$−$NADP^+$ (Figure 2)] of the enzyme. The W697H and S698Δ mutants elicited the fastest k_{obs1} rate constants (115 and 82 s^{-1}, respectively), which are 4−5-fold faster than those of the native enzyme and the S698A mutant.[27] The corresponding k_{obs1} for W697S (3 s^{-1}) is 8-fold slower than that of the native enzyme.

As in wild-type MSR, the second kinetic phase (conversion of B to C) in the Ser mutants corresponds to the E−$FADH_2$−FMN complex being partially converted to the disemiquinone state (E−$FADH^{\bullet}$−$FMNH^{\bullet}$) of the enzyme, following transfer of a single electron from $FADH_2$ to FMN. Formation of this intermediate is spectrally evident as a simultaneous decrease in absorbance at 454 nm and a buildup of a spectral band centered at 600 nm (Figure 5A,B). The observed rate constant (k_{obs2}) for B to C conversion is 2.3 s^{-1} for S689A and 2.0 s^{-1} for S698Δ (10-fold faster than that of wild type). Like that of the wild type, conversion of C to D in S698A and S698Δ is associated with reduction of MSR to the four-electron-reduced state by a second molecule of NADPH, and the observed rate constants (k_{obs3}) are similar to that of the native enzyme (0.02 s^{-1}). Transient disemiquinone formation is also observed for S689A and S689Δ with an initial increase followed by a decrease in absorbance at 600 nm over 100 s (insets of panels A and B of Figure 5).

In contrast to the S698 mutants and the native enzyme,[27] global analysis of SVD-transformed data does not show transient formation of a broad absorbance band at 600 nm during NADPH-catalyzed flavin reduction of the W697 mutants (Figure 5C,D). The absence of a detectable disemiquinone intermediate is also evident by the lack of an absorbance change at 600 nm over 100 s (insets of panels C and D of Figure 5). Thus, for W697H and W697S, conversion of B to C represents full four-electron reduction of the enzyme by a second molecule of NADPH, and the associated rate constants for this final phase are 0.008 and 0.005 s^{-1}, respectively.

The final absorbance spectra of W697H and W697S show that both mutants can be reduced to the four-electron level (E−$FADH_2$−$FMNH_2$) in the presence of excess NADPH. This observation coupled with the ability of both mutants to catalyze cytochrome c^{3+} reduction (a reaction that is dependent on the

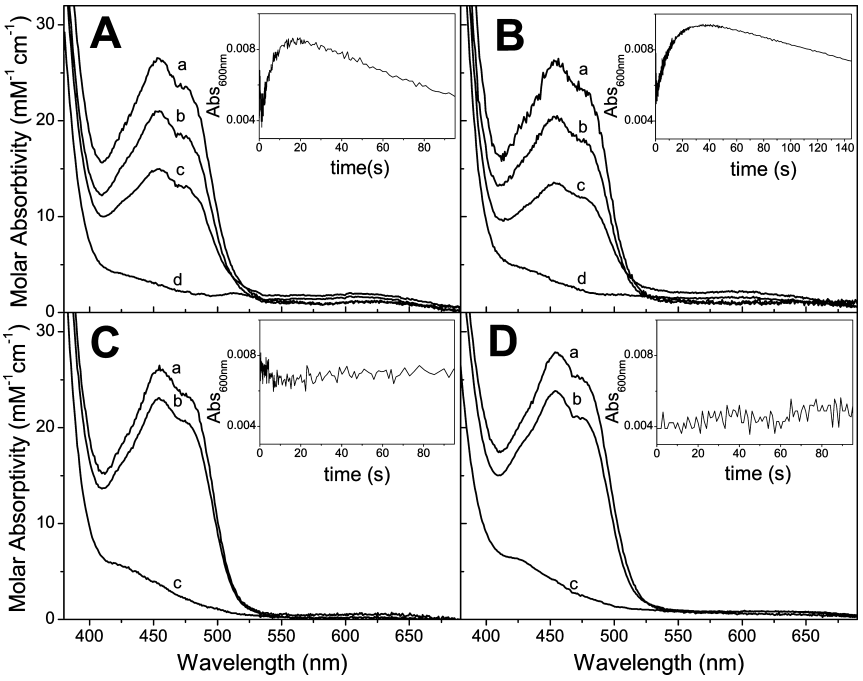

Figure 5. Resolved spectral intermediates following rapid mixing of MSR variants (20 μM) with NADPH (200 μM). Reaction conditions are detailed in Experimental Procedures. The time-dependent spectral changes in the flavin absorbance were monitored by stopped-flow photodiode array spectroscopy from 200 to 500 s. The spectral data were subject to SVD and global fitting; the deconvoluted spectral intermediates resulting from the analysis are displayed. For the (A) S698A and (B) S698Δ variants, the time-resolved spectral data were best fit to a three-step model with four intermediates (A → B → C → D), while the (C) W697H and (D) W697S variants accommodate a two-step model with three discrete spectral species (A → B → C). The calculated observed rate constants for the interconversion of spectral intermediates are listed in Table 2. Insets of panels A–D are stopped-flow absorbance traces at 600 nm following mixing of MSR variants (20 μM) with NADPH under pseudo-first-order conditions.

Table 2. Observed Rate Constants for NADPH-Catalyzed Reduction of MSR Variants

enzyme	k_{obs1} (s^{-1})	k_{obs2} (s^{-1})	k_{obs3} (s^{-1})
wild type[a]	24.9 ± 0.1	0.18 ± 0.010	0.016 ± 0.003
S698A[b]	27.2 ± 0.3	2.33 ± 0.01	0.025 ± 0.001
S698Δ	82.1 ± 0.7	2.01 ± 0.04	0.019 ± 0.001
enzyme	k_{obs1} (s^{-1})	k_{obs2} (s^{-1})	
W697H	115.3 ± 0.6	0.008 ± 0.001	
W69S	3.4 ± 0.1	0.011 ± 0.001	

[a]Data from ref 27. [b]Observed rate constants were determined by global analysis of SVD-transformed time-resolved spectral data as described in Experimental Procedures. The data for W697H and W697S mutants were best fit to a two-kinetic phase reaction model, whereas data for all other mutants and wild-type MSR were best fit to a three-kinetic phase reaction model.

transfer of an electron from the FMN domain) suggests that they are still able to mediate interflavin electron transfer, but at an attenuated rate. To confirm that this is the case, we generated the two-electron-reduced state of the W697 mutants by rapidly mixing the enzyme with an equimolar amount of NADPH. Over a 750 s time frame, there was a decrease in absorbance at 454 nm accompanied by an increase at 600 nm. These changes in absorbance spectra reflect the disproportionation of electrons between the flavins as the W697H and W697S equilibrate to the disemiquinone state (Figure 6). Thus, the absence of a detectable disemiquinone intermediate following rapid mixing of the enzyme with NADPH under pseudo-first-conditions reflects attenuation, as opposed to the abolishment of $FADH_2$ to FMN electron transfer in the W697 mutants.

Single-Wavelength Stopped-Flow Analysis of Flavin Reduction. Single-wavelength stopped-flow experiments were performed under pseudo-first-order conditions in which the NADPH concentration was in >7-fold excess over the enzyme concentration. Flavin reduction was monitored under anaerobic conditions following an absorbance decrease at 454 nm (Figure 7). Stopped-flow traces over a 10 s time domain were fit to a double-exponential equation (eq 2), yielding observed rate constants. The first observed rate constant, which reports on the first hydride transfer event, closely matches that obtained from global analysis of PDA data (Figure 5), with W697H eliciting the fastest observed rate (136 s^{-1}) followed by S698Δ (106 s^{-1}), S898A (23 s^{-1}), and W697S (3.5 s^{-1}). For the S698A and S698Δ mutants, a fit of the double-exponential equation to the single-wavelength data over 10 s yielded k_{obs2} values of 1.6 s^{-1} for S698A and 3.7 s^{-1} for S698Δ, which are similar to the values obtained from PDA analysis (Table 2). For W697S and W679H mutants, the second kinetic phase is incomplete over 10 s, and hence, k_{obs2} generates values of 0.20 and 0.26 s^{-1}, respectively, which do not match that obtained from multiwavelength stopped-flow analysis (Table 2). However, a fit of a double exponential to the absorbance trace over 500 s generated a k_{obs2} of 0.005 s^{-1} for both mutants (insets of panels C and D of Figure 7), similar to the k_{obs2} in Table 2.

Wild-type MSR elicited a hyperbolic dependence of k_{obs1} on NADPH concentration.[27] The stopped-flow data for the native enzyme (shown in ref 27) were fit to a hyperbolic function that was derived from a two-step binding mechanism in which rapid binding of NADPH is followed by a slow isomerization step (e.g., displacement of W697), generating an apparent dissociation constant (K_d) of 37–60 μM.[27] In this study, k_{obs1}

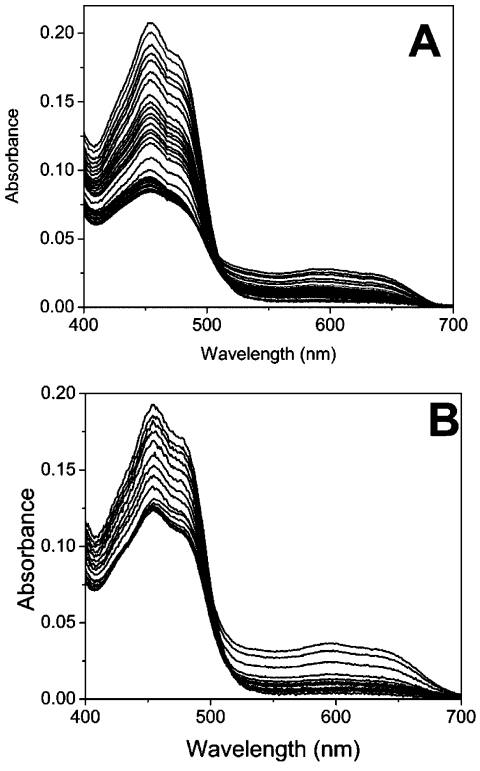

Figure 6. Reduction of W679 MSR variants by NADPH to the two-electron-reduced state. Absorbance spectra from 700 to 300 nm were recorded by photodiode array spectroscopy following rapid mixing of 16 μM W697H (A) and W697S (B) with NADPH (16 μM). The time-dependent spectral changes over 750 s show a decrease in the absorbance maxima at 454 nm and an increase in absorbance at 600 nm. For the sake of clarity, only select spectra are shown.

was independent of NADPH concentration for all four MSR variants, suggesting that the reduced coenzyme binds more tightly than the native enzyme (Figure 8). These data are consistent with product inhibition studies, which show tighter binding for $NADP^+$ in each of the four mutants. Although it is not known if the oxidized and reduced coenzymes bind with the same affinities to the MSR variants, evidence suggests that they are similar for the native enzyme. Support for this comes from stopped-flow analysis in which the reverse rate constant for the transfer of a hydride from the two-electron-reduced FNR domain of MSR to $NADP^+$ was also shown to be hyperbolically dependent on $NADP^+$ concentration, yielding an apparent dissociation constant similar to that of NADPH (~55 μM).[27] This apparent K_d for $NADP^+$ is comparable to the K_i for $NADP^+$ (37 μM) determined from product inhibition and the dissociation constant determined through ITC experiments.[31] Collectively, this suggests that the K_i values for $NADP^+$ not only report on the binding affinity of $NADP^+$ but also reflect relative binding affinities of NADPH. Thus, the lack of a dependence of k_{obs1} on NADPH concentration combined with lower observed inhibition constants for $NADP^+$ indicates that binding of the NADP(H) is tighter in all four mutants.

Coenzyme Preference. Like other members of the diflavin oxidoreductase family, MSR shows a strong specificity preference for NADPH over NADH as a reducing coenzyme (19000-fold).[31] Mutation of the FAD aromatic stacking residue to a smaller residue (Ser, Ala, or His) in CPR,[30] NOSred,[39] and FNR[40,41] led to a dramatic reduction in coenzyme preference as judged by the coenzyme specificity ratio $[(k_{cat}/K_{NADPH})/(k_{cat}/K_{NADH})]$, revealing that the bulky side chain does dictate a large part of the enzyme's specificity for the 2′-phosphorylated coenzyme. Table 3 confirms that W697 also helps discriminate against NADH, as the coenzyme preference decreased to 1264-fold for W697H and 21-fold for W697S.

DISCUSSION

The role of the FAD aromatic stacking residue in NADPH-dependent flavoproteins has been the subject of intensive kinetic and structural analyses. The residue can be either a tryptophan as in the case of MSR, CPR, NR1, and P450BM3, a phenylalanine in the isoforms of NOSred, or tyrosine for spinach FNR (Figure 3). Previous studies with this class of enzymes showed that selective mutagenesis of the aromatic FAD stacking residue improved binding of the nicotinamide mononucleotide (NMN) portion of the coenzyme, supporting the hypothesis that conformational movement of this aromatic side chain is required for hydride transfer.[32,33] This was confirmed through crystallographic structures of enzyme variants in which the FAD aromatic residue was deleted or substituted with a smaller side chain.[32,33] The structures revealed that the nicotimamide ring (usually disordered in the native enzyme) was at a 30° angle with respect to the *re* face of the isoalloxazine ring, in position for transfer of the *pro-R* hydrogen from C4 of the nicotinamide ring to N5 of the isoalloxazine ring. Despite the fact that the structures indicate that the coenzyme could readily adopt a catalytically productive conformation, mutation of this bulky aromatic residue to a small side chain typically resulted in attenuated rates of catalysis (see refs 30 and 32−34).[a] In contrast, we observe disparate effects on catalysis with the four MSR variants; W697H and S698Δ elicited 5−6-fold increases in the observed rate constant of hydride transfer, accompanied by more modest increases in the rate of steady-state cytochrome c^{3+} turnover. S698A, on the other hand, exhibited catalytic properties similar to those of the wild type, while W697S elicited pronounced decreases in both steady-state turnover and pre-steady-state rates of hydride and interflavin electron transfer. A detailed analysis of the kinetic properties of the four MSR variants alongside analogous mutants of human CPR has provided new insight into the role of the highly conserved aromatic FAD-stacking residue in mediating intraprotein electron transfer.

Control of Coenzyme Binding and Preference. Isothermal titration calorimetry, stopped-flow, and steady-state inhibition assays with wild-type MSR showed tighter binding of 2′,5′-ADP (1 μM) than of NADP(H) (37−60 μM).[31] These differences in binding affinity, which are acute for MSR compared to related flavoproteins, are attributed to the bipartite binding nature of the coenzyme, first described for FNR.[32] The substrate analogue, 2′,5′-ADP, binds more tightly than $NADP^+$ because the binding energy of the coenzyme is largely attributed to a number of electrostatic interactions between the 2′-phosphate and charged residues in the coenzyme binding cleft. Moreover, the nicotinamide mononucleotide (NMN) half of the coenzyme clashes with the active site residues, disrupting formation of the MSR−NADP(H) complex. As a result, the pyridine nucleotide is envisioned to bind in a two-step process in which initial anchoring of the 2′,5′-ADP moiety is followed by productive binding of the nicotinamide ring adjacent to the FAD isoalloxazine ring for hydride transfer.

Steady-state inhibition data for $NADP^+$ and 2′,5′-ADP indicate that the C-terminal mutations have a more profound

dx.doi.org/10.1021/bi2012228 | *Biochemistry* 2011, 50, 11131−11142

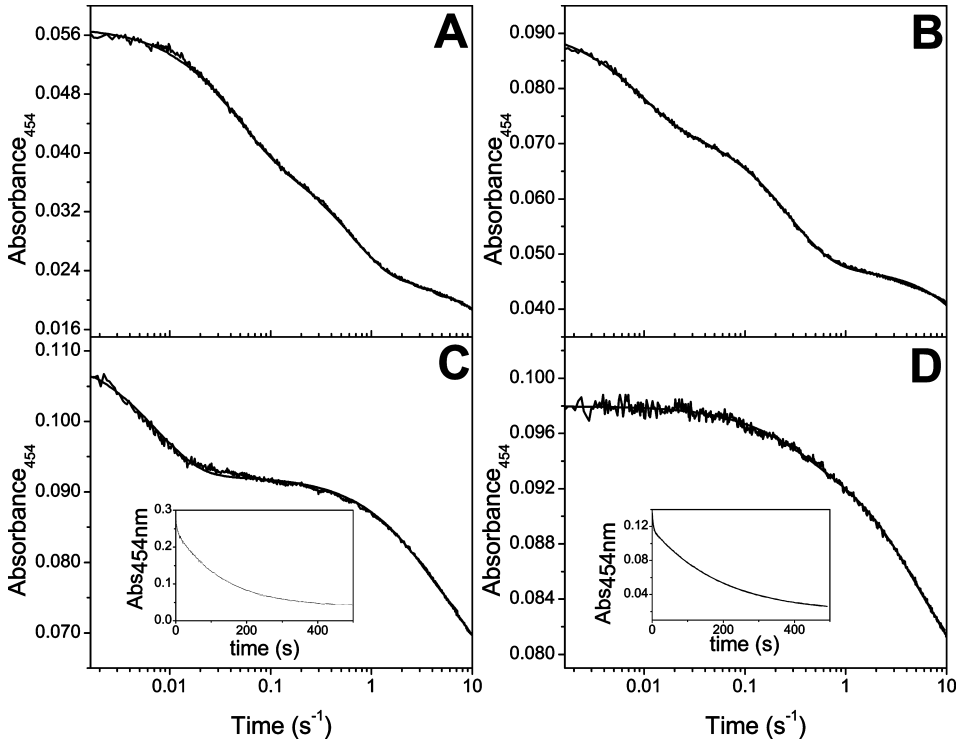

Figure 7. Stopped-flow single-wavelength absorbance (454 nm) traces following mixing of MSR variants (8 μM) with NADPH under pseudo-first-order conditions. Fitting of data in panels A (S698A), B (S698Δ), C (W697H), and D (W697S) to a double exponential gave k_{obs1} values of 22.8 ± 0.2 (A, S698A), 106.5 ± 0.9 (B, S698Δ), 135.8 ± 2.0 (C, W697H), and 3.5 ± 0.2 (D, W697S) and k_{obs2} values of 1.6 ± 0.0 (A), 3.7 ± 0.02 (B), 0.26 ± 0.01 (C), and 0.20 ± 0.01 (D), respectively. The insets in panels C and D are absorbance traces over 500 s. A fit of the trace to a double-exponential equation yields a k_{obs2} of 0.005 s^{-1} for both W697 mutants.

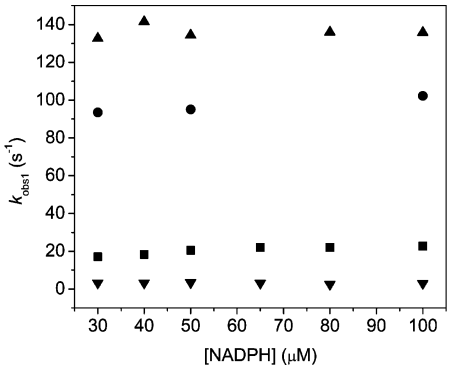

Figure 8. Dependence of k_{obs1} on the concentration of NADPH for S698A (■), S698Δ (●), W796H (▲), and W697S (▼).

effect on NMN binding, as the $NADP^+$ K_i values were highly varied (in particular for the W697 variants) compared to the inhibition constants for 2′,5′-ADP. Of the four variants, W697H elicits a relatively large K_i for $NADP^+$ (only 1.5-fold smaller than that of native MSR) compared to the K_i of 2′,5′-ADP, suggesting that the imidazole ring can partially substitute for the bulky indole side chain in contributing to the unfavorable energetics of NMN binding. Thus, in W697H and to a lesser degree in the S698 mutants, the bipartite binding nature of the pyridine nucleotide is maintained, but the energetic cost for productive placement of the NMN portion of the coenzyme is reduced, as all three mutants elicit lower K_i values for $NADP^+$ than for the wild type. Conversely, $NADP^+$ binds more tightly compared to 2′,5′-ADP in W697S. Mutation of W697 to a small polar residue likely creates a water-filled cavity next to the *re* face of FAD, and this is expected to favor hydrophobic interaction between the nicotinamide ring of the incoming NADPH and the isoalloxazine ring. The increase in affinity for the NMN moiety in W697S likely disrupts the inherent two-step binding mechanism, as docking of the coenzyme can be driven by this favorable hydrophobic interaction. This difference in binding mode may also explain why W697S loses its strong preference for NADPH over NADH. The role of the 2′-phosphate in anchoring of the coenzyme to the binding cleft, a process that likely acts to discriminate against NADH binding, may be superseded by favorable interactions between FAD and the nicotinamide ring. Analogous mutations in related flavoproteins have had similar effects on coenzyme preference.[30,39,41]

Table 3. Kinetic Constants for MSR-Catalyzed Reduction of Cytochrome c^{3+} with NADH

MSR	k_{cat} (s^{-1})	K_m ($\times 10^{-3}$ M)	k_{cat}/K_m ($\times 10^{-3}$ M^{-1} s^{-1})	$(k_{cat}/K_{NADPH})/(k_{cat}/K_{NADH})$
W697S	7.96 ± 0.40	0.06 ± 0.01	122.5 ± 30.7	21
W697H	4.74 ± 0.90	4.47 ± 0.42	0.94 ± 0.27	1264
wild type[a]	0.24 ± 0.03	3.53 ± 0.56	0.068 ± 0.014	19400

[a]Data from ref 31.

dx.doi.org/10.1021/bi2012228 | *Biochemistry* 2011, 50, 11131–11142

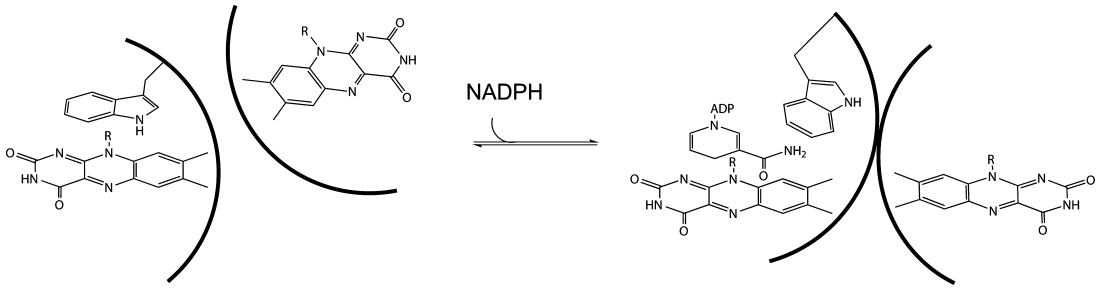

Figure 9. Model for the action of Trp697 in facilitating interflavin electron transfer in the flipped out conformation, by forming a favorable contact with the FMN domain.

Control of Hydride Transfer. Stopped-flow analysis revealed that W697H and S698Δ elicited a 5−6-fold increase in k_{obs1}, the first kinetic phase of flavin reduction. The observed rate constant, k_{obs1} encompasses the initial steps of the kinetic mechanism: diffusion of NADPH into the active site, displacement of W697 by NADPH, and the first hydride transfer step to FAD (steps 1−3, respectively, of Figure 2). Thus, an overall increase in k_{obs1} can arise from the mutations accelerating one or more of these steps of the mechanism. Given the extensive $\pi-\pi$ stacking between the indole ring of W697 and the FAD isoalloxazine ring observed in the crystal structure of the MSR FNR module,[31] displacement of this residue by the nicotinamide moiety likely constitutes an energetic barrier for productive NADPH binding and hydride transfer. If this conformational switch within the active site is rate-limiting for k_{obs1} and is tightly coupled to subsequent hydride transfer, then lowering of the energy barrier for displacement of W697 will result in faster rates for this first kinetic phase. Swapping the indole ring for an imidazole side chain reduces the $\pi-\pi$ interaction with FAD and possibly the thermodynamic barrier for displacement of the residue by NADPH. The crystal structure of MSR FNR (or full-length CPR) reveals that the C-terminal S698 residue is not restrained through electrostatic interactions or hydrogen bonds to neighboring residues; thus, simultaneous movement of both S698 and W697 likely contributes to the energetic cost for productive NADPH binding.[20] Hence, deletion of the C-terminal residue in S698Δ possibly reduces the steric constraint for movement of the penultimate residue, translating into faster rates of hydride transfer. The fact that S698A elicits a k_{obs1} similar to that of wild-type MSR indicates that the complete C-terminal residue, minus the Cβ hydroxyl moiety, energetically restricts rotation of W697.

Conversely, the W697S mutation showed an 8-fold decrease in k_{obs1}, despite a perceived reduction in the energetic barrier for catalytic positioning of the nicotinamide ring. The attenuation in the rate of hydride transfer may arise from disruption of bipartite binding of the coenzyme observed for this mutant. Initial anchoring of the coenzyme by the 2′,5′-ADP half of the molecule may restrict movement of the NMN moiety, which may in turn reduce the extent of localized searching for the optimal distance and orientation for transfer of a hydride between C4 of the nicotinamide ring and N5 of FAD. In other words, the attenuated rate for k_{obs1} may arise from enhanced conformational freedom of the NMN moiety as it binds to the active site. Alternatively, the W697S mutation may significantly affect the redox potentials of the FAD cofactor, making hydride transfer less thermodynamically favorable. This seems unlikely given that removal of this aromatic stacking residue likely exposes the FAD to the solvent, which is expected to lower the reduction potential of the cofactor. This in turn would thermodynamically favor reduction of FAD by NADPH, increasing the rate of hydride transfer.[25] Indeed, mutation of an analogous tryptophan to an alanine or histidine in P450BM3 resulted in a more electropositive $FAD_{ox/hq}$ couple.[42]

Control of Interflavin Electron Transfer. Analysis of multiwavelength and single-wavelength stopped-flow data reveals that NADPH reduction of the W697H and W697S mutants to the four-electron-reduced state occurs without the observable (and transient) formation of the disemiquinone intermediate, which would otherwise signify FAD to FMN electron transfer (step 4 of Figure 2). Nevertheless, the fact that both W697H and W697S are still able to (i) catalyze cytochrome c^{3+} reduction, (ii) reduce to the four-electron state under pseudo-first-order conditions, and (iii) equilibrate to the disemiquinone state upon being mixed with an equimolar amount of NADPH, indicates that the electrons still disproportionate between the flavins. Thus, W697, while not essential for FAD to FMN electron transfer, does accelerate this step of catalysis, which in the wild-type enzyme and Ser698 variants results in the observable accumulation of the disemiquinone intermediate.

We propose that W697, once displaced by the nicotinamide ring of the incoming NADP(H), stabilizes the compact conformational substate of the enzyme, thereby increasing the rate of FAD to FMN electron transfer. Diflavin oxidoreductases, by virtue of the highly mobile FMN domain, are envisioned to adopt different conformational substates during catalysis. In the compact substate, captured in the first crystal structure of rat CPR,[20] there is close interfacial contact between the flavin domains and alignment of the two isoalloxazine rings such that they form a continuous sheet. This configuration of the flavins is anticipated to allow for rapid and direct electron transfer between the cofactors. In the open state, observed in subsequent crystal structures of CPR variants, the FMN domain dissociates from the FNR module and is rotated as much as 60° for the delivery of an electron to the physiological electron acceptor.[24] Toggling between the open and compact state allows the FMN to accept an electron from FAD and subsequently donate it to an external electron acceptor. Given that W697 is located near the FNR and FMN binding interface,[31] it is reasonable to speculate that displacement of the W697 indole ring by the nicotinamide of NADPH may cause the side chain to rotate toward the FMN domain and form part of the binding interface between the flavin domains. In its "flipped out" conformation, W697 may act to stabilize the domain interface and shift the conformational equilibrium of the enzyme to the compact substate, which would increase the probability and rate of interflavin electron transfer (Figure 9).

If the new role of the aromatic stacking were extended to CPR, it would explain why a W676H human CPR mutant results in attenuated rates of FAD reduction[34] and cytochrome c^{3+} turnover,[30] whereas an analogous mutation in MSR leads to accelerated rates of catalysis. For full-length CPR, which also elicits multiphasic flavin reduction, the initial observed rate of FAD reduction (k_{obs1}), which encompasses the hydride transfer step, is 20 s^{-1}.[43] For the full-length CPR W676H mutant and the isolated FNR-like module of CPR, the corresponding rate constant decreases to 3 s^{-1}.[34] In contrast, k_{obs1} is ~25 s^{-1} for full-length MSR and its isolated FNR component.[27] The difference in the observed rate constants of FAD reduction for the isolated FNR modules of CPR and MSR can be explained in part by differences in the midpoint potentials of the $FAD_{ox/hq}$ couple. The $FAD_{ox/hq}$ couple is 80 mV more electronegative in CPR (−340 mV) than in MSR (−260 mV); thus, delivery of a hydride ion from NADPH (redox couple of −320 mV) to FAD is less thermodynamically favorable[36,44] for the former enzyme, which is reflected by the slower rate constant of 3 s^{-1} for the isolated FNR module of CPR.

Why then are the observed rates of FAD reduction (k_{obs1}) similar between the full-length forms of MSR and CPR? For CPR, subsequent interflavin transfer of an electron to the higher-potential $FMN_{ox/sq}$ likely accelerates the observed rate of hydride transfer in CPR and explains why the isolated CPR FNR module shows diminished rates of hydride transfer. In MSR, which elicits relatively slow rates of interflavin electron transfer, a more electropositive $FAD_{ox/hq}$ couple contributes to the observed rate constant for hydride transfer, which is supported by the fact that the isolated FNR domain and full-length MSR have the same observed rate constant for this kinetic step. Therefore, if the indole ring of the FAD stacking tryptophan accelerates the transfer of an electron between the FAD and FMN (presumably in its flipped out conformation), one would expect that mutation of this residue would diminish the observed rates of hydride transfer in CPR, but not MSR. Thus, while a W697H mutation in MSR slows FAD to FMN electron transfer, it will not impede hydride transfer (k_{obs1} is in fact accelerated), because the former kinetic step is not tightly coupled to the latter step. In contrast, the W676H mutation in CPR reduces the observed rate of hydride transfer, because disruption of the transfer of an electron to the more electropositive FMN cofactor affects the thermodynamics of hydride transfer as the potential of the $FAD_{ox/hq}$ couple is more electronegative than that of the NADPH/$NADP^+$ couple.

NMR, small-angle X-ray scattering, and ELDOR spectroscopy provide evidence that the family of diflavin oxidoreductases adopts a heterogeneous mixture of conformational substates in solution and further indicate that coenzyme binding pulls the dynamic equilibrium toward the compact state.[45−47] Temperature-jump experiments have also shown that binding of $NADP^+$ to CPR enhances interflavin electron transfer, possibly because of modification of this conformational equilibrium.[48] The structural basis for coenzyme binding favoring the compact state of the enzyme may be linked to the intermittent rotation of the penultimate residue toward the FMN domain. In support of this model are the crystal structures of a W677 deletion mutant of full-length CPR, which show an increased level of disorder for the FMN domain with $NADP^+$ bound.[33]

There is the possibility that the penultimate Trp acts as an electron conduit between the flavins. This seems unlikely given that the edge-to-edge distance between the FAD and FMN isoalloxazine rings is 4 Å in the compact state of the CPR. The proximity of the flavins allows the electron to tunnel unaided from one redox center to the next. For MSR, in which conformational movement between the flavin cofactors is heightened (supported by reduced rates of interflavin electron transfer, extended hinge region, and lack of an air-stable semiquinone), W697 may still act in a manner analogous to that proposed for CPR and partially restrict FMN domain movement when the coenzyme is bound. The fact that the W697 mutants are still capable of mediating interflavin electron transfer reinforces a model in which the tryptophan is not a molecular switch that turns on and off electron transfer but rather accelerates the transfer of electrons between the cofactors. Indeed, this new role for the FAD stacking tryptophan may extend to other diflavin oxidoreductases (NR1 and P450BM3) in which the FAD aromatic stacking residue is also an indole ring.[a] The abundance of smaller aromatics (e.g., Tyr) in NADPH-dependent FAD enzymes (i.e., the FNR superfamily) suggests that the indole ring is a structural adaptation that coevolved with the fusion of bacterial FNR- and FMN-containing flavodoxins.

For W697H and S698Δ, only a modest increase in k_{cat} for cytochrome c^{3+} reduction was observed, despite a 5−10-fold increase in the rates of uncoupled NADPH oxidation and hydride transfer. The k_{cat} for cytochrome c^{3+} reduction is a product of all of the forward rate constants of the catalytic mechanism, including NADPH binding, hydride transfer, interflavin electron transfer, and $NADP^+$ release. Therefore, in W697H, the faster rates of hydride transfer, coupled with diminished rates of FAD to FMN electron transfer and relatively weak $NADP^+$ binding, result in a combination of forward rate constants that leads to an only modest increase in k_{cat}. For S698Δ, which elicited fast rates of hydride and interflavin electron transfer, the overall slight increase in the rate of cytochrome c^{3+} turnover may instead arise from relatively tight binding of $NADP^+$ (18-fold tighter than that of the native enzyme). This likely leads to the formation of a stronger MSR−$NADP^+$ complex, resulting in slow dissociation of the oxidized coenzyme for the next round of catalysis.[30]

Concluding Remarks. From our mutagenesis studies, we conclude that W697 is an important control point for coenzyme binding and catalysis in MSR. W697 presents an energetic barrier for catalytic positioning of the nicotinamide ring of NADPH, which in turn attenuates FAD reduction. While placement of this conserved aromatic residue against the FAD isoalloxazine ring seems counterproductive for efficient catalysis, its position is critical for anchoring of the 2′,5′-ADP portion of the coenzyme prior to productive binding of the nicotinamide ring. This bipartite binding of the coenzyme allows the enzyme to discriminate against NADH and may also restrict movement of the NMN moiety, allowing for faster alignment with the FAD isoalloxazine ring for hydride transfer. W697 also accelerates interflavin electron transfer. Structurally this may manifest itself by W697 bridging the FMN and FNR domain interface in the flipped out conformation, which favors alignment of the redox centers for efficient intraprotein electron transfer. These studies not only widen our understanding of structure−function relationships within the family of diflavin oxidoreductases but also may shed new light on the importance of MSR in maintaining MS function.

AUTHOR INFORMATION

Corresponding Author

*Department of Chemistry, University of British Columbia, 3333 University Way, Kelowna, BC, Canada V1V 1V7. Phone: (250) 807-8663. Fax: (250) 807-8009. E-mail: kirsten.wolthers@ubc.ca.

Funding

This work is supported by a grant from the Natural Sciences and Engineering Research Council of Canada and the U.K. Biotechnology and Biological Sciences Research Council (BBSRC). N.S.S. is a BBSRC Professorial Research Fellow and a Royal Society Wolfson Merit Award holder.

ABBREVIATIONS

MSR, methionine synthase reductase; MS, methionine synthase; FAD, flavin adenine dinucleotide; FMN, flavin mononucleotide; NADPH, reduced nicotinamide adenine dinucleotide phosphate; NADH, reduced nicotinamide adenine dinucleotide; $NADP^+$, oxidized nicotinamide adenine dinucleotide phosphate; 2′,5′-ADP, 2′,5′-adenosine diphosphate; ox/sq, oxidized/semiquinone; ox/hq, oxidized/hydroquinone; sq/hq, semiquinone/hydroquinone; CPR, cytochrome P450 reductase; NOSred, reductase domain of nitric oxide synthase; NR1, NADPH-dependent oxidoreductase; LB, Luria Broth; Tris, tris(hydroxymethyl)aminomethane; P450BM3, *Bacillus megaterium* flavocytochrome; NMN, nicotinamide mononucleotide; FNR, ferredoxin $NADP^+$-reductase; SVD, singular-value decomposition; MetH, *E. coli* cobalamin-dependent methionine synthase; NMR, nuclear magnetic resonance; ELDOR, electron−electron double resonance.

ADDITIONAL NOTE

[a]The exceptions are the nitric oxide synthases, which elicit complex flavin reduction kinetics that is dependent on a number of unique control elements.

REFERENCES

(1) Drummond, J. T., Huang, S., Blumenthal, R. M., and Matthews, R. G. (1993) Assignment of enzymatic function to specific protein regions of cobalamin-dependent methionine synthase from *Escherichia coli*. *Biochemistry 32*, 9290−9295.

(2) Tang, K. H., Chang, C. H., and Frey, P. A. (2001) Electron transfer in the substrate-dependent suicide inactivation of lysine 5,6-aminomutase. *Biochemistry 40*, 5190−5199.

(3) Padovani, D., and Banerjee, R. (2006) Assembly and protection of the radical enzyme, methylmalonyl-CoA mutase, by its chaperone. *Biochemistry 45*, 9300−9306.

(4) Kajiura, H., Mori, K., Tobimatsu, T., and Toraya, T. (2001) Characterization and mechanism of action of a reactivating factor for adenosylcobalamin-dependent glycerol dehydratase. *J. Biol. Chem. 276*, 36514−36519.

(5) Mori, K., Bando, R., Hieda, N., and Toraya, T. (2004) Identification of a reactivating factor for adenosylcobalamin-dependent ethanolamine ammonia lyase. *J. Bacteriol. 186*, 6845−6854.

(6) Banerjee, R. V., and Matthews, R. G. (1990) Cobalamin-dependent methionine synthase. *FASEB J. 4*, 1450−1459.

(7) Olteanu, H., and Banerjee, R. (2001) Human methionine synthase reductase, a soluble P-450 reductase-like dual flavoprotein, is sufficient for NADPH-dependent methionine synthase activation. *J. Biol. Chem. 276*, 35558−35563.

(8) Wolthers, K. R., Toogood, H. S., Jowitt, T. A., Marshall, K. R., Leys, D., and Scrutton, N. S. (2007) Crystal structure and solution characterization of the activation domain of human methionine synthase. *FEBS J. 274*, 738−750.

(9) Leclerc, D., Wilson, A., Dumas, R., Gafuik, C., Song, D., Watkins, D., Heng, H. H., Rommens, J. M., Scherer, S. W., Rosenblatt, D. S., and Gravel, R. A. (1998) Cloning and mapping of a cDNA for methionine synthase reductase, a flavoprotein defective in patients with homocystinuria. *Proc. Natl. Acad. Sci. U.S.A. 95*, 3059−3064.

(10) Wilson, A., Leclerc, D., Rosenblatt, D. S., and Gravel, R. A. (1999) Molecular basis for methionine synthase reductase deficiency in patients belonging to the cblE complementation group of disorders in folate/cobalamin metabolism. *Hum. Mol. Genet. 8*, 2009−2016.

(11) Wald, D. S., Law, M., and Morris, J. K. (2002) Homocysteine and cardiovascular disease: Evidence on causality from a meta-analysis. *BMJ [Br. Med. J.] 325*, 1202−1209.

(12) Clarke, R., Smith, A. D., Jobst, K. A., Refsum, H., Sutton, L., and Ueland, P. M. (1998) Folate, vitamin B12, and serum total homocysteine levels in confirmed Alzheimer disease. *Arch. Neurol. 55*, 1449−1455.

(13) van der Put, N. M., van Straaten, H. W., Trijbels, F. J., and Blom, H. J. (2001) Folate, homocysteine and neural tube defects: An overview. *Exp. Biol. Med. 226*, 243−270.

(14) van der Linden, I. J., den Heijer, M., Afman, L. A., Gellekink, H., Vermeulen, S. H., Kluijtmans, L. A., and Blom, H. J. (2006) The methionine synthase reductase 66A>G polymorphism is a maternal risk factor for spina bifida. *J. Mol. Med. 84*, 1047−1054.

(15) Wilson, A., Platt, R., Wu, Q., Leclerc, D., Christensen, B., Yang, H., Gravel, R. A., and Rozen, R. (1999) A common variant in methionine synthase reductase combined with low cobalamin (vitamin B12) increases risk for spina bifida. *Mol. Genet. Metab. 67*, 317−323.

(16) Elmore, C. L., Wu, X., Leclerc, D., Watson, E. D., Bottiglieri, T., Krupenko, N. I., Krupenko, S. A., Cross, J. C., Rozen, R., Gravel, R. A., and Matthews, R. G. (2007) Metabolic derangement of methionine and folate metabolism in mice deficient in methionine synthase reductase. *Mol. Genet. Metab. 91*, 85−97.

(17) Deng, L., Elmore, C. L., Lawrance, A. K., Matthews, R. G., and Rozen, R. (2008) Methionine synthase reductase deficiency results in adverse reproductive outcomes and congenital heart defects in mice. *Mol. Genet. Metab. 94*, 336−342.

(18) Jarrett, J. T., Hoover, D. M., Ludwig, M. L., and Matthews, R. G. (1998) The mechanism of adenosylmethionine-dependent activation of methionine synthase: A rapid kinetic analysis of intermediates in reductive methylation of cob(II)alamin enzyme. *Biochemistry 37*, 12649−12658.

(19) Fujii, K., Galivan, J. H., and Huennekens, F. M. (1977) Activation of methionine synthase: Further characterization of flavoprotein system. *Arch. Biochem. Biophys. 178*, 662−670.

(20) Wang, M., Roberts, D. L., Paschke, R., Shea, T. M., Masters, B. S., and Kim, J. J. (1997) Three-dimensional structure of NADPH-cytochrome P450 reductase: Prototype for FMN- and FAD-containing enzymes. *Proc. Natl. Acad. Sci. U.S.A. 94*, 8411−8416.

(21) Bredt, D. S., Hwang, P. M., Glatt, C. E., Lowenstein, C., Reed, R. R., and Snyder, S. H. (1991) Cloned and expressed nitric oxide synthase structurally resembles cytochrome P-450 reductase. *Nature 351*, 714−718.

(22) Paine, M. J., Garner, A. P., Powell, D., Sibbald, J., Sales, M., Pratt, N., Smith, T., Tew, D. G., and Wolf, C. R. (2000) Cloning and characterization of a novel human dual flavin reductase. *J. Biol. Chem. 275*, 1471−1478.

(23) Haque, M. M., Panda, K., Tejero, J., Aulak, K. S., Fadlalla, M. A., Mustovich, A. T., and Stuehr, D. J. (2007) A connecting hinge represses the activity of endothelial nitric oxide synthase. *Proc. Natl. Acad. Sci. U.S.A. 104*, 9254−9259.

(24) Hamdane, D., Xia, C. W., Im, S. C., Zhang, H. M., Kim, J. J. P., and Waskell, L. (2009) Structure and Function of an NADPH-Cytochrome P450 Oxidoreductase in an Open Conformation Capable of Reducing Cytochrome P450. *J. Biol. Chem. 284*, 11374−11384.

(25) Murataliev, M. B., Feyereisen, R., and Walker, F. A. (2004) Electron transfer by diflavin reductases. *Biochim. Biophys. Acta 1698*, 1−26.

(26) Stuehr, D. J., Tejero, J., and Haque, M. M. (2009) Structural and mechanistic aspects of flavoproteins: Electron transfer through the nitric oxide synthase flavoprotein domain. *FEBS J. 276*, 3959−3974.
(27) Wolthers, K. R., and Scrutton, N. S. (2004) Electron transfer in human methionine synthase reductase studied by stopped-flow spectrophotometry. *Biochemistry 43*, 490−500.
(28) Gutierrez, A., Grunau, A., Paine, M., Munro, A. W., Wolf, C. R., Roberts, G. C., and Scrutton, N. S. (2003) Electron transfer in human cytochrome P450 reductase. *Biochem. Soc. Trans. 31*, 497−501.
(29) Welland, A., and Daff, S. (2010) Conformation-dependent hydride transfer in neuronal nitric oxide synthase reductase domain. *FEBS J. 277*, 3833−3843.
(30) Dohr, O., Paine, M. J. I., Friedberg, T., Roberts, G. C. K., and Wolf, C. R. (2001) Engineering of a functional human NADH-dependent cytochrome P450 system. *Proc. Natl. Acad. Sci. U.S.A. 98*, 81−86.
(31) Wolthers, K. R., Lou, X., Toogood, H. S., Leys, D., and Scrutton, N. S. (2007) Mechanism of coenzyme binding to human methionine synthase reductase revealed through the crystal structure of the FNR-like module and isothermal titration calorimetry. *Biochemistry 46*, 11833−11844.
(32) Deng, Z., Aliverti, A., Zanetti, G., Arakaki, A. K., Ottado, J., Orellano, E. G., Calcaterra, N. B., Ceccarelli, E. A., Carrilli, N., and Karplus, P. A. (1999) A productive $NADP^+$ binding mode of ferredoxin-$NADP^+$ reductase revealed by protein engineering and crystallographic studies. *Nat. Struct. Biol. 6*, 847−853.
(33) Hubbard, P. A., Shen, A. L., Paschke, R., Kasper, C. B., and Kim, J. J. (2001) NADPH-cytochrome P450 oxidoreductase. Structural basis for hydride and electron transfer. *J. Biol. Chem. 276*, 29163−29170.
(34) Gutierrez, A., Doehr, O., Paine, M., Wolf, C. R., Scrutton, N. S., and Roberts, G. C. (2000) Trp-676 facilitates nicotinamide coenzyme exchange in the reductive half-reaction of human cytochrome P450 reductase: Properties of the soluble W676H and W676A mutant reductases. *Biochemistry 39*, 15990−15999.
(35) Konas, D. W., Zhu, K., Sharma, M., Aulak, K. S., Brudvig, G. W., and Stuehr, D. J. (2004) The FAD-shielding residue Phe1395 regulates neuronal nitric-oxide synthase catalysis by controlling $NADP^+$ affinity and a conformational equilibrium within the flavoprotein domain. *J. Biol. Chem. 279*, 35412−35425.
(36) Wolthers, K. R., Basran, J., Munro, A. W., and Scrutton, N. S. (2003) Molecular dissection of human methionine synthase reductase: Determination of the flavin redox potentials in full-length enzyme and isolated flavin-binding domains. *Biochemistry 42*, 3911−3920.
(37) Vangelder, B. F., and Slater, E. C. (1962) Extinction Coefficient of Cytochrome C. *Biochim. Biophys. Acta 58*, 593.
(38) Wolthers, K. R., and Schimerlik, M. I. (2002) Neuronal nitric oxide synthase: Substrate and solvent kinetic isotope effects on the steady-state kinetic parameters for the reduction of 2,6-dichloroindophenol and cytochrome c^{3+}. *Biochemistry 41*, 196−204.
(39) Konas, D. W., Zhu, K., Sharma, M., Aulak, K. S., Brudvig, G. W., and Stuehr, D. J. (2004) The FAD-shielding residue Phe(1395) regulates neuronal nitric-oxide synthase catalysis by controlling $NADP^+$ affinity and a conformational equilibrium within the flavoprotein domain. *J. Biol. Chem. 279*, 35412−35425.
(40) Piubelli, L., Aliverti, A., Arakaki, A. K., Carrillo, N., Ceccarelli, E. A., Karplus, P. A., and Zanetti, G. (2000) Competition between C-terminal tyrosine and nicotinamide modulates pyridine nucleotide affinity and specificity in plant ferredoxin-$NADP^+$ reductase. *J. Biol. Chem. 275*, 10472−10476.
(41) Tejero, J., Perez-Dorado, I., Maya, C., Martinez-Julvez, M., Sanz-Aparicio, J., Gomez-Moreno, C., Hermoso, J. A., and Medina, M. (2005) C-terminal tyrosine of ferredoxin-$NADP^+$ reductase in hydride transfer processes with $NAD(P)^+$/H. *Biochemistry 44*, 13477−13490.
(42) Neeli, R., Roitel, O., Scrutton, N. S., and Munro, A. W. (2005) Switching pyridine nucleotide specificity in P450 BM3: Mechanistic analysis of the W1046H and W1046A enzymes. *J. Biol. Chem. 280*, 17634−17644.
(43) Gutierrez, A., Lian, L. Y., Wolf, C. R., Scrutton, N. S., and Roberts, G. C. (2001) Stopped-flow kinetic studies of flavin reduction in human cytochrome P450 reductase and its component domains. *Biochemistry 40*, 1964−1975.
(44) Munro, A. W., Noble, M. A., Robledo, L., Daff, S. N., and Chapman, S. K. (2001) Determination of the redox properties of human NADPH-cytochrome P450 reductase. *Biochemistry 40*, 1956−1963.
(45) Hay, S., Brenner, S., Khara, B., Quinn, A. M., Rigby, S. E., and Scrutton, N. S. (2010) Nature of the energy landscape for gated electron transfer in a dynamic redox protein. *J. Am. Chem. Soc. 132*, 9738−9745.
(46) Rigby, S. E., Lou, X., Toogood, H. S., Wolthers, K. R., and Scrutton, N. S. (2011) ELDOR spectroscopy reveals that energy landscapes in human methionine synthase reductase are extensively remodelled following ligand and partner protein binding. *ChemBioChem 12*, 863−867.
(47) Ellis, J., Gutierrez, A., Barsukov, I. L., Huang, W. C., Grossmann, J. G., and Roberts, G. C. (2009) Domain motion in cytochrome P450 reductase: Conformational equilibria revealed by NMR and small-angle X-ray scattering. *J. Biol. Chem. 284*, 36628−36637.
(48) Gutierrez, A., Munro, A. W., Grunau, A., Wolf, C. R., Scrutton, N. S., and Roberts, G. C. (2003) Interflavin electron transfer in human cytochrome P450 reductase is enhanced by coenzyme binding. Relaxation kinetic studies with coenzyme analogues. *Eur. J. Biochem. 270*, 2612−2621.